Biosensors and Bioelectronics 155 (2020) 112115

Contents lists available at ScienceDirect

Biosensors and Bioelectronics

journal homepage: http://www.elsevier.com/locate/bios

Upconversion nanoparticle-mOrange protein FRET nanoprobes for self-ratiometric/ratiometric determination of intracellular pH, and single cell pH imaging

Sandip Ghosh [a], Yu-Fen Chang [b], De-Ming Yang [a,c], Surojit Chattopadhyay [a,*]

[a] Institute of Biophotonics, National Yang-Ming University, 155 Sec-2, Li Nong Street, Taipei, 112, Taiwan
[b] LumiStar Biotechnology Inc., National Biotechnology Research Park, Taipei, 115, Taiwan
[c] Microscopy Service Laboratory, Basic Research Division, Department of Medical Research, Taipei Veterans General Hospital, Taipei, 112, Taiwan

ARTICLE INFO

Keywords:
Upconversion nanoparticles
mOrange fluorescent proteins
Intracellular pH
FRET
Nanoprobe
Nano-biosensor

ABSTRACT

Fluorescence based intracellular pH nanoprobes have been developed that overcomes the limitations imposed by shallow penetration depth of ultraviolet excitation, photostability, phototoxicity, and interference from background autofluorescence. In this study, we have constructed a Förster Resonance Energy Transfer (FRET) based pH nanoprobe using upconversion nanoparticle (UCNP) as a donor (excitation/emission @ 980/540 nm, green channel), and mOrange fluorescent protein (excitation/emission @ 548/566 nm, red channel) as acceptor. The UCNP-mOrange nanoprobe could be fluorescently imaged with 980 nm excitation, having deep penetration depth, by a fluorescence microscope on a coverslip, or uptaken in a single HeLa cell. The cellular upatake of these nanoparticles were confirmed by transmission electron microscope study. The FRET probes, with a FRET efficiency of ~20% at physiological pH of 7.0, have simultaneous self-ratiometric and ratiometric features varying linearly with local pH. The probe exhibits high accuracy, sensitivity, reversibility, and stability over a wide range of pH (3.0–8.0). The fluorescence intensity ratio from individual green, and red channels in fluorescence microscopic images could be used to estimate the pH of the intracellular compartments of HeLa cell from the pH dependent ratiometric calibration. Nigericin mediated intracellular pH (3.0, 5.0, and 7.0) could be accurately estimated from the CLSM derived FRET ratio. The pH probes demonstrate high stability and reversibility when switched between pH 3, and 8 for at least 5 cycles.

1. Introduction

pH in an intracellular matrix plays an important role in controlling cellular signal transduction (Clark et al., 1999; Golovina and Blaustein, 1997), enzymatic activities (Han and Burgess, 2010), cell growth and apoptosis (Gottlieb and Dosanjh, 1996; Loiselle and Casey, 2003), cell metabolism (Loiselle and Casey, 2003), ion transporting (Zhao et al., 1995), endocytosis (Yuli and Oplatka, 1987), and even cell adhesion (Chun and Jacobson, 1993). Alteration of intracellular pH may lead to dysfunction in a cell. Most importantly, abnormal pH may cause or indicate cancer (Webb et al., 2011), neurological problem (e.g., Alzheimer's disease) (Davies et al., 1993), and other fatal diseases (Kellum, 2000). Therefore, intracellular pH is a primary indicator of cell health that needs to be monitored as diagnostic tools. The pH can also be used as a trigger for drug release/delivery approaches within a cell (Duan and Nie, 2007). Electrode or probe based pH monitoring is easy for samples and solutions available in the bulk. The measurement becomes challenging inside a cell and hence the need for fluorescence based probes.

Several techniques, including H^+ permeable microelectrodes (Wray, 1988), Raman spectroscopy (Kneipp et al., 2007; Talley et al., 2004), absorption spectroscopy (Dennis et al., 2012), fluorescence spectroscopy and imaging (Dennis et al., 2012; Gert-Jan Kremers and Davidson; Li et al., 2016; Llopis et al., 1998) have drawn attention for monitoring/measuring intracellular pH. Among all, fluorescence imaging based technique requires simple sample preparation and has better sensitivity (Li et al., 2016; Näreoja et al., 2017), and most importantly, can be performed noninvasively. Among these fluorescence based techniques, employment of Förster Resonance Energy Transfer (FRET) is most common (Arppe et al., 2014; Chen et al., 2012) as it enables to have both ratiometric (Näreoja et al., 2017), and self-ratiometric measurements (Li

* Corresponding author.
E-mail address: sur@ym.edu.tw (S. Chattopadhyay).

https://doi.org/10.1016/j.bios.2020.112115
Received 10 December 2019; Received in revised form 5 February 2020; Accepted 19 February 2020
Available online 26 February 2020

et al., 2016) described later. In a typical FRET 'donor-acceptor' nanoprobe construct, at least one is pH sensitive and is a pH indicator (Arppe et al., 2014). pH sensitive organic dyes (Li et al., 2016), or pH sensitive fluorescent proteins (FP) (Dennis et al., 2012) are generally used. Fluorophores like FPs (Llopis et al., 1998), quantum dots (QDs) (Dennis et al., 2012), carbon nanodots (Shi et al., 2012), and upconversion nanoparticles (UCNPs) are used (Li et al., 2016; Näreoja et al., 2017). Dennis et al., (2012) demonstrated a FRET based nanoprobe using QD, and mOrange FPs for ratiometric intracellular pH sensing. In another recent study by Tuomas et al. (Näreoja et al., 2017), UCNPs and polymer based FRET probe is used for intracellular pH sensing. However, these probes suffer from inherent problems such as short excitation wavelength of donor, penetration depth, rapid photobleaching of pH indicating dyes, cellular toxicity, stability, and sensitivity. In addition, none of the FRET probes are designed to have simultaneous ratiometric, and self-ratiometric measurement of intracellular pH. Therefore, to overcome the intrinsic problems a new class of probe has to be constructed.

In this work, we have constructed a UCNP ($NaGdF_4$:Yb^{3+}, Er^{3+}) donor, and pH sensitive mOrange FP acceptor as a novel FRET probe for intracellular pH sensing. As the UCNPs are excited in the infrared (IR), this probe can overcome all the mentioned difficulties in terms of providing a better penetration depth, photostability, minimum background autofluorescence, minimum photobleaching, biocompatibility, and reversibility. Most importantly, these nanoprobes can have simultaneous ratiometric and self-ratiometric measurements of intracellular pH.

2. Experimental

2.1. Materials

For the synthesis of the oleic acid capped $NaGdF_4$:Yb^{3+},Er^{3+} UCNPs, $GdCl_3$, $YbCl_3$, $ErCl_3$, Oleic acid (OA), 1-octadecene (ODE), ammonium fluoride (NH_4F), NaOH and analytical grade chemicals, such as ethanol, cyclohexane, and methanol were all purchased from Sigma Aldrich, USA.

For the citrate coating on UCNPs, diethylene glycol (DEG) (Vetec chemical, USA), sodium citrate dehydrate (JT Baker, USA), chloroform and toluene (Alfa Aesar, UK), and hydrochloric acid were purchased and used as received.

2.2. Synthesis of OA capped upconversion nanoparticles (UCNPs)

The Yb^{3+}/Er^{3+}-doped $NaGdF_4$ nanocrystals were prepared by thermal decomposition method as reported previously by Liu et al., (2013). Typically, $GdCl_3$ (80%), $YbCl_3$ (18%), $ErCl_3$ (2%) were first mixed with 14 mL of OA and 16 mL of ODE in a 100 mL three-necked flask. The resultant mixture was then heated to 150 °C under nitrogen atmosphere to form a homogeneous solution. When the above solution is cooled down to 50 °C, 10 mL of methanol solution containing NaOH (2.5 mmol) and NH_4F (4 mmol) is added drop by drop while stirring for 30 min. Subsequently, methanol in the system was removed by keeping the reaction system at 100 °C. Later, the mixture was heated to 300 °C for 1 h under flowing nitrogen, and then cooled down to room temperature (25–26 °C). The resultant precipitate containing the UCNPs were washed with ethanol 5 times and finally redispersed in cyclohexane until next use.

2.3. Surface modification of UCNPs by citric acid ligand (Cit-UCNPs)

For surface-ligand exchange reaction, we followed a standard chemical route as reported previously by Cao et al., (2010). In this synthesis process, DEG (15 mL) and sodium citrate dehydrate (588.2 mg) were mixed for 45 min with a speed of 500 rpm, and then heated to 110 °C for 40 min under a continuous flow of Ar gas. Afterwards, 10 mg of OA capped UCNPs were dispersed in a solution containing chloroform and toluene (3:2 v/v) were injected into the above reaction chamber, and heated to 160 °C. After the chloroform and toluene had evaporated, the reaction chamber was re-heated up to 220 °C for 3 h. Later, the reaction was terminated by cooling down to room temperature. The resultant solution was then treated with 0.1 M HCl solution, and the products were subsequently precipitated. The precipitates were collected by centrifugation (14000 rpm, 15 min) and washed three times with ethanol and deionized (DI) water, and redispersed in DI water.

2.4. Expression, amplification, and purification of mOrange fluorescent proteins (FPs)

The His6-tagged mOrange FPs were derived from pRSET-b mOrange plasmid. mOrange proteins were expressed in *E. coli* (BL21) competent cells. Later, we lysed the bacterial cell membrane, by performing mechanical lysis, using mechanical probe sonicator. Finally, we collected the proteins after centrifugation of the sample. To purify the as obtained proteins, we used His GraviTrap purification kit (GE Health care, Sweden). The detailed experimental steps are shown schematically in the Electronic Supporting Information (Fig. S1, ESI) and a step-by-step protocol can be found in the ESI. The purity of the as-obtained mOrange FPs is investigated via SDS-PAGE gel electrophoresis (Wurtele and Nikolau, 2000).

2.5. Construction of Cit-UCNP-mOrange FRET nanoprobes (UCMF)

The Cit-UCNP-mOrange FRET nanoprobes (UCMF) were constructed via EDC (1-ethyl-3-(3-dimethylaminopropyl) carbadimide) (Sigma Aldrich, USA) chemistry (Dennis et al., 2012). For the probe construction, we have used 2 mL of Cit-UCNPs (1.5 mg mL^{-1}) with 2 mL of mOrange FPs (0.35 mg mL^{-1}), and 3 mL of EDC (6 mg mL^{-1}) were incubated overnight at 4 °C with gentle shaking (200 rpm). By-products, such as free UCNPs, excess mOrange FPs, and unreacted EDC were removed using a centrifugation filter device with a 100 kDa molecular weight cutoff (PALL, USA).

2.6. Characterisation of UCNPs, Cit-UCNPs, and UCMF

The optical absorption spectra of as-synthesized materials were recorded by UV–Vis–NIR spectrometer (Jasco V770, USA) in the range of 200–2700 nm. Fluorescence spectra were recorded by a Fluorolog spectrophotometer (JY Fluorolog 3 with iHR 320, Horiba, Japan), equipped with a 980 nm cw laser excitation (SDL, China). The surface charge of all the materials used, including the nanocomposites, was measured with a Zeta potential machine (NanoPlus Particulate System, USA). The morphology and crystal structures were imaged by High Resolution Transmission Electron Microscope (HR-TEM, JEM-2010F, JEOL, Japan).

To examine cellular internalization of the nanoprobes, we preformed bio-TEM on the HeLa cells. The HeLa cells were dispensed into a 10 cm dish at a concentration of 10^6 cells/well and incubated for 24 h for cell attachment. Thereafter, UCMFs were added to the above dish at a concentration of 200 ppm. After 24 h of incubation, the cells were washed at least three times with PBS, trypsinized, centrifuged, fixed, dehydrated, and embedded in resin. Subsequent to resin hardening, the block was sectioned with a ultramicrotome (Leica EM UC7, Germany) to allow electron transparency. Several of these sections (with embedded cells) were observed by TEM.

For the FRET imaging, we have used an inverted fluorescence microscope (Zeiss Axiovert 200) equipped with a 980 nm cw laser (CNI, China), and compatible optics and a wide-view dual-mode CMOS camera (Hamamatsu, Japan) to record high resolution images.

2.7. Spectroscopic FRET (pH dependent) measurement of UCMF

The spectral characteristics of the UCMF nanoprobe were measured

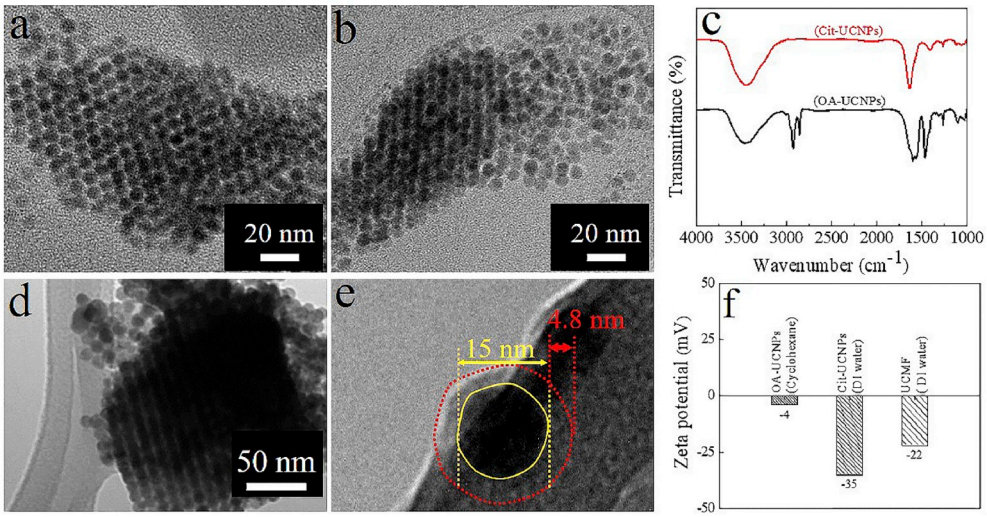

Fig. 1. Morphology, and surface properties of as-synthesized nanoparticle nanoprobes. TEM images of (a) OA-UCNPs, (b) Cit-UCNPs. (c) FTIR spectra of OA-UCNPs, and Cit-UCNPs. (d) TEM image of UCMF. (c) HR-TEM image of a single UCMF. The yellow circle with solid line shows the single upconversion nanoparticle, and mOrange fluorescent proteins (red circle with dashed line). (d) Zeta potentials of OA-UCNPs, Cit-UCNPs, and UCMF. (For interpretation of the references to colour in this figure legend, the reader is referred to the Web version of this article.)

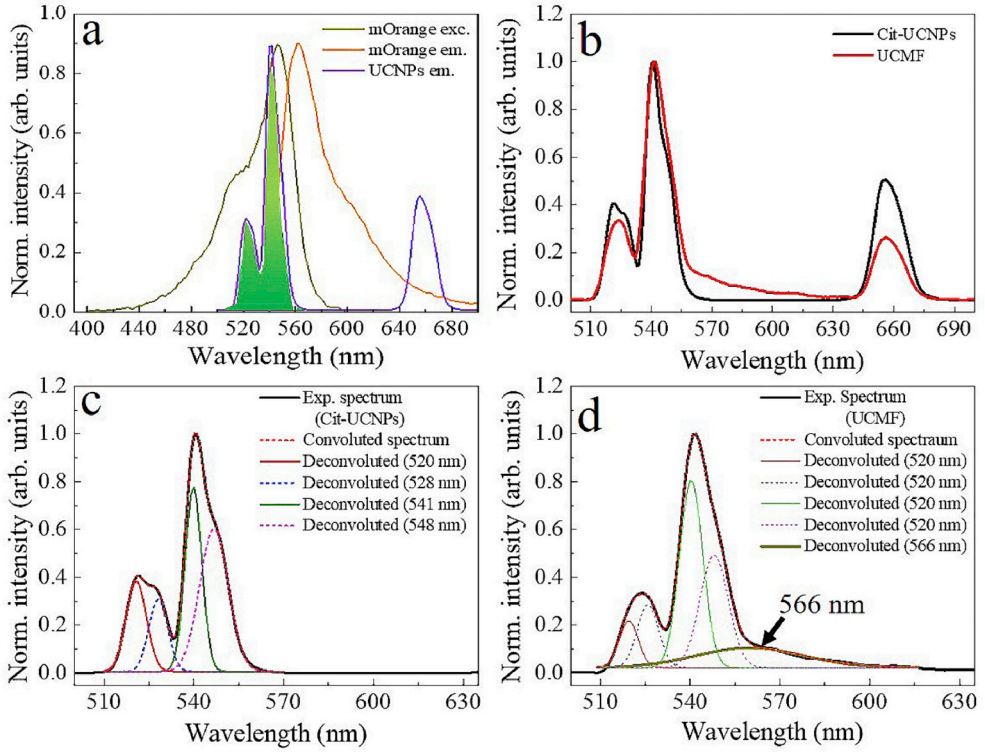

Fig. 2. FRET characterisations of UCMF. (a) Spectral overlapping between the emission of FRET donor (Cit-UCNPs), excitation of FRET acceptor (mOrange FPs). (b) Upconversion fluorescence emission and FRET emission spectra of Cit-UCNPs, and UCMF, respectively. (c) Deconvolution of the emission spectrum of Cit-UCNPs, under illumination with 980 nm laser. (d) Deconvolution of the FRET emission spectrum of UCMF, which shows a sensitized emission band at 566 nm (black arrow), and is coming from mOrange FPs.

over a range of pH (3–8) by mixing 200 μL of probe with 800 μL of 20 mM phosphate-buffered saline (PBS)/citrate buffer with adjusted different pH values. The FRET emission spectra were measured with the Fluorolog spectrophotometer with excitation at 980 nm. To evaluate the reversibility of pH sensing, UCMF were dispersed into buffered solution and the pH of the solution was changed from pH = 3.0 to 8.0, and vice versa for five pH cycles using 1 M HCl and 1 M of NaOH. Later, from the measured fluorescence spectra we obtained the self-ratiometric, and ratiometric calibration curves as a function of pH.

2.8. FRET ratio imaging and in-vitro pH calibration of UCMF

After completion of the spectroscopic study, we performed imaging of the as-prepared UCMF FRET nanoprobes under a FRET ratio imaging system. To get the in-vitro or in-cell epi-fluorescent signals of UCMF FRET nanoprobes, namely the UCNP and mOrange, the FRET ratio image system (Chiu and Yang, 2012) was used with some modifications. Briefly, it is equipped with a 980 nm laser, and a mercury lamp as excitation sources, an inverted microscope (Axiovert 200M, Zeiss) with a 60x oil objectives (NA = 1.45, Olympus, Japan), and a shutter with a dichroic mirror, and an emission filter to block the 980 nm NIR leak. A Wide-View module (Gemini, Hamamatsu; with filters ET530/40X nm for UCNP and ET600/75 nm for mOrange and a T560lpxr-UF1 nm dichroic mirror), a CMOS camera (ORCA-Flash4.0 LT, Hamamatsu, Japan), and a software (HCImage, Hamamatsu, Japan) was used to conduct the FRET ratio image capture procedure. The emission signals, either UCNP (510–550 nm in the green channel) and mOrange (560–630 nm in the red channel) were acquired simultaneously under

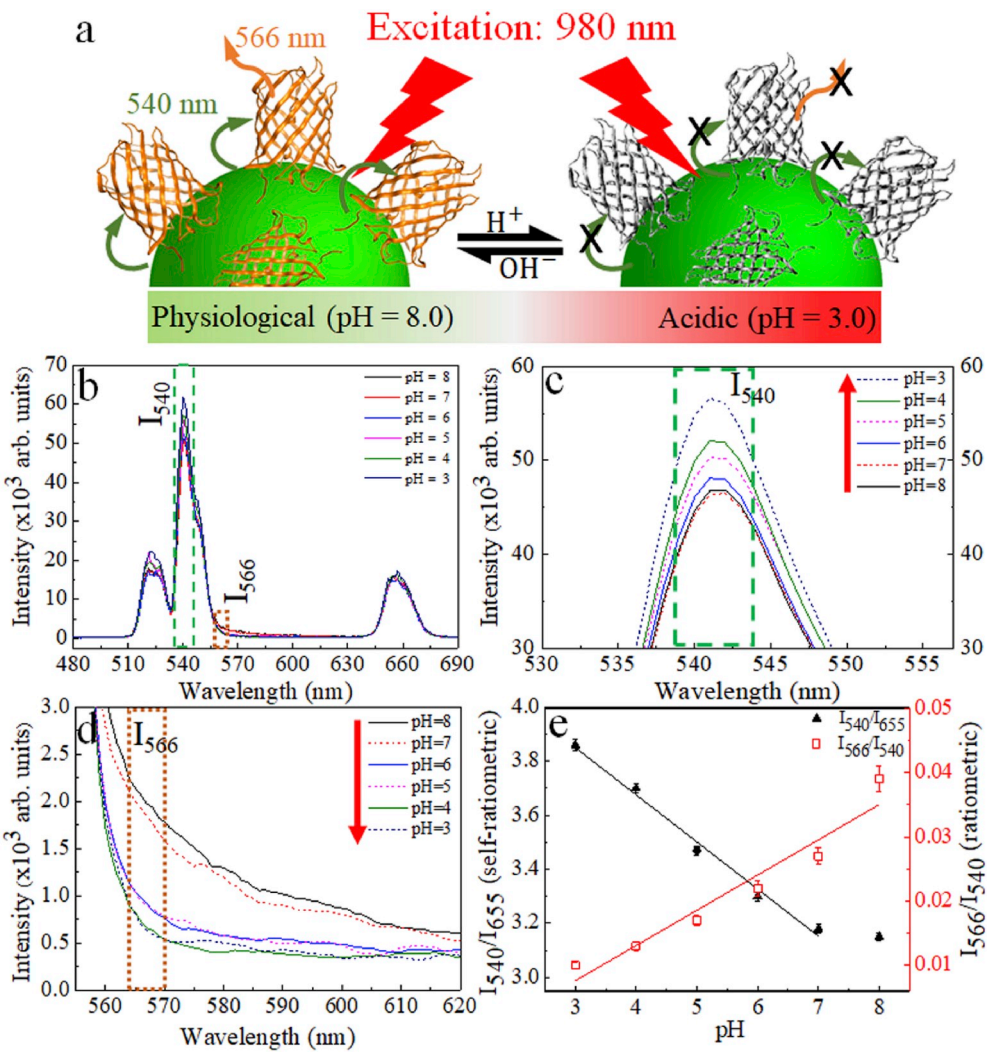

Fig. 3. pH dependent FRET measurements of UCMF. (a) Schematic demonstration of the pH dependent energy transfer between the Cit-UCNP (FRET donor), and mOrange FPs (FRET acceptor). In an alkaline environment, energy transfer (ET) from FRET donor to FRET acceptor is maximum, resulting in decrease in UCNP emission, whereas the ET is zero at acidic environment. (b) pH dependent fluorescence emission spectra of UCMF, under the illumination with 980 nm light. (c) Enhanced spectra (green dashed box in Fig. 3b) for the UCNPs emission. (d) Enhanced spectra (orange dashed box in Fig. 3b) for the mOrange FPs emission. (e) The self-ratiometric (donor emission only, I_{540} to I_{655}), and ratiometric (acceptor emission, at 566 nm (I_{540}) to donor emission, at 540 nm (I_{540})), analysis as a function of pH. The line joining the data points is a linear fit. The adjacent R^2 for self-ratiometric, and ratiometric fitting is 0.98, and 0.94, respectively. (For interpretation of the references to colour in this figure legend, the reader is referred to the Web version of this article.)

the excitation of the 980 nm laser. 10 μL of nanoprobe solution was dropped on a thin glass coverslip, and the FRET images were recorded. To obtain the pH calibration curve, we have diluted the UCMFs into different pH buffered solution and dropped on a glass coverslip to record the FRET images.

2.9. Cell cytotoxicity of UCMF via MTT assay

To check cellular toxicity of these UCMFs, the MTT assay (Chen et al., 2019) was performed. HeLa cells were cultured in DMEM media (with 10% fetal bovine serum, and 1% penicillin, streptomycin). Later, HeLa cells were seeded in a 96-well plate at a density of 10000 cells/well and incubated for 24 h at 37 °C under 5% CO_2. Then, 150 μL of concentration controlled (0, 50, 100, 200, 400 ppm) UCMF (diluted in DMEM media) were added to the culture medium, each concentration being repeated in five parallel wells ($n = 5$). After being incubated for 24 h, the cells were washed twice with 1x PBS, and then 150 μL of 3-(4,5-dimethylthiazol-2-yl)-2,5-diphenyltetrazolium (MTT-Sigma Aldrich, USA) was added into each well and incubated for another 4–5 h. Subsequently, the media was removed and the formed formazan crystals were dissolved in 150 μL dimethyl sulfoxide (DMSO, Sigma Aldrich, USA). To quantify the cell viability, the optical density at 570 nm of each well was recorded by an ELISA multiplate reader (TECAN, Switzerland).

2.10. Intracellular FRET imaging

To acquire the live cellular FRET images, HeLa cells (10000 cells/well) were cultured and seeded in a 29 mm glass bottom dish (Cellvis, USA) for 24 h at 37 °C, and 5% CO_2. 100 μL of UCMF (200 ppm) solution were added to the above dish. After 24 h of incubation, the dish was washed twice with 1x PBS. Then the HeLa cells, with the UCMFs, were taken for FRET ratio imaging. For in situ calibrations of the pH nanoprobes, intracellular pH was adjusted to that of the extracellular pH environment controlled by an ionophore 'Nigericin' (481990, Calbiochem, Merck, USA). Nigericin would enforce ion diffusion through the cell membrane to ensure the same pH inside the cell as the extracellular medium which can be measured easily with a pH meter. For this purpose, HeLa cells (with UCMFs) were washed and incubated in pH (3.0, 5.0, and 7.0) controlled citrate/phosphate buffer medium. Afterwards, each well was treated with 20 μM of Nigericin (Li et al., 2016; Näreoja et al., 2017) and incubated for 30 min at 37 °C, and 5% CO_2.

3. Results and discussions

3.1. Structural morphology and surface characterisation of OA-UCNPs, Cit-UCNPs, and UCMF

We begin with the morphological characterisation of the as-synthesized UCNPs used in this study. Fig. 1a shows the hexagonal morphology of the OA-UCNPs prepared by thermal decomposition

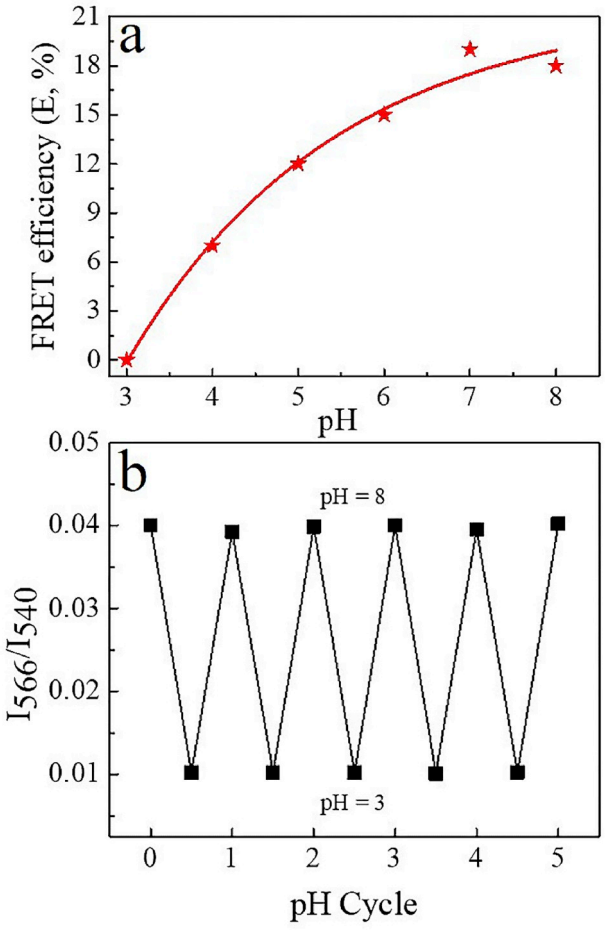

Fig. 4. FRET analysis. (a) FRET efficiency of UCMF over the relevant pH range (3–8). (b) The ratio of the relative emission intensity I_{540}/I_{566} (excited with 980 nm laser) when pH varied with HCl and NaOH solutions from 3.0 to 8.0, repeatedly over 5 cycles. The lines joining the data points are a guide to the eye only.

method (Chen et al., 2014a). Fig. 1a shows nearly monodispersed UCNPs with an average diameter of 15 ± 2 nm. However, these OA-UCNPs is usually dispersed in cyclohexane, and therefore cannot be used in biological studies. In such cases, the surface ligand of the as-prepared OA-UCNPs, can be exchanged for biocompatibility. In this case, we have adopted the ligand exchange strategy to remove the oleic acid with citric acid (Cit-UCNPs). Since the ligand exchange reaction is performed at relatively elevated temperature (220 °C), it is important to investigate the Cit-UCNP shape and size. Fig. 1b shows the uniform distribution of Cit-UCNPs. The overall size (15 ± 2 nm) of these Cit-UCNPs remain unchanged from the OA-UCNPs and are chemically stable.

For the confirmation of complete replacement of OA by –COOH on the UCNP surface, we have done Fourier-transform infrared (FTIR) spectroscopy of the two UCNPs sample, OA-UCNPs, and Cit-UCNPs (Fig. 1c) (Cao et al., 2010; Xu et al., 2016). The broad transmission dip at 3450 cm^{-1} for both the OA- and Cit-UCNPs can be attributed to the O–H stretching vibration (Hu et al., 2009). The transmission dips at ~2930, and ~2854 cm^{-1} for OA-UCNPs can be assigned to the asymmetric, and symmetric stretching of CH_2 group in the long alkyl chain (Hu et al., 2009). The dip at 3008 cm^{-1} is attributed to the = C–H stretching vibration. The features near ~2930, and 2854 cm^{-1} coming from the OA-ligands are missing in the Cit-UCNP spectrum, indicating complete replacement by –COOH. In addition, bands at 1553, and 1458 cm^{-1} corresponding to asymmetric and symmetric stretching of the carboxylic group, respectively, marked its presence (Hu et al., 2009).

FRET probe, UCMF, formed using Cit-UCNPs and mOrange FPs have been constructed via EDC mediated chemical route (Dennis et al., 2012). In principle, EDC act as a cross linker that would activate a covalent amide bonding between carboxyl terminated group from the citric acid ligand (attached to the UCNPs), and the N-terminal of the mOrange FPs. Fig. 1d shows a fashioned array of UCMFs with a uniform size distribution. Fig. 1e shows the higher magnification TEM of a single UCMF. Under TEM, UCNPs appears in dark (yellow circle), and mOrange proteins appeared with a poor contrast due to low electron density in the proteins (Chen et al., 2014b; Liu et al., 2017). The overall size of the UCMFs has increased to 25 ± 0.5 nm because of the mOrange protein shell of 4.8 ± 0.5 nm thickness around the UCNPs (Shu et al., 2006).

The surface charge of OA-UCNPs, Cit-UCNPs, and UCMFs was measured and compared. The Zeta potential for OA-UCNPs (in hexane), Cit-UCNPs, and UCMFs (in water) is −4 (Lü et al., 2008), −35 (Lü et al., 2008; Wilhelm et al., 2015), and −22 mV (Brewer et al., 2005), respectively (Fig. 1f). The changes in surface potential further confirmed the successful surface modification and protein conjugation on the UCMFs.

3.2. Optical properties of OA-UCNPs, Cit-UCNPs, and UCMF

Figure S2 (ESI) represent the optical absorption and upconversion emission characteristics of the UCNPs, before and after surface modification. Fig. S2a shows the UV–Vis–NIR absorption spectra of UCNPs, and Cit-UCNPs with a feature at ~980 nm for both OA-UCNPs and Cit-UCNPs (Chen et al., 2014a). The slight decrease in the absorption strength in the Cit-UCNPs may have occurred due to various reasons, including change in solvent type (Boyer et al., 2010; Sedlmeier and Gorris, 2015), refractive indices of solvent (Toptygin et al., 2002), collisional quenching (Lakowicz, 2006), dopant ions leakage during surface modification (Boyer et al., 2010), and so on. Fig. S2b shows optical photographs of colloidal solutions containing OA-UCNPs (in cyclohexane), and Cit-UCNPs (in DI water) emitting green light when illuminated with 980 nm laser. Figure S2c,d (ESI) shows the power-dependent upconversion emission spectra of OA-UCNPs, and Cit-UCNPs, respectively. The characteristic emission bands of the OA-UCNPs and Cit-UCNPs appeared at 365, 408, 520, 540, and 655 nm (Figs. S2c and d, ESI) (Chen et al., 2014a; Huang et al., 2013) due to the Er^{3+} (emitter) doping. In addition, the upconversion fluorescence emission intensity (I) increased with increasing illumination power.

Table 1
Comparison of characteristics of different FRET probes for intracellular pH sensing.

Probe type	Exc. (nm)	Penetration depth	Donor QY (%)	FRET efficiency (%)	Sensitivity (Ratiometric)	Sensitivity (Self-ratiometric)	Ref.
UCNP-FITC	980	deep	5	–	–	3.56/pH	Li et al. (2016)
UCNP-pHrodo	980	deep	5	–	0.34/pH	–	Näreoja et al. (2017)
QD-mOrange	400	shallow	~80	50 (pH ~7)	0.32/pH	–	Dennis et al. (2012)
UCNP- pHrodo	980	deep	5	–	0.04/pH	–	Arppe et al. (2014)
UCNP-mOrange	980	deep	5	20 (pH ~7)	0.01/pH	0.17/pH	This work.

- indicates values not reported.

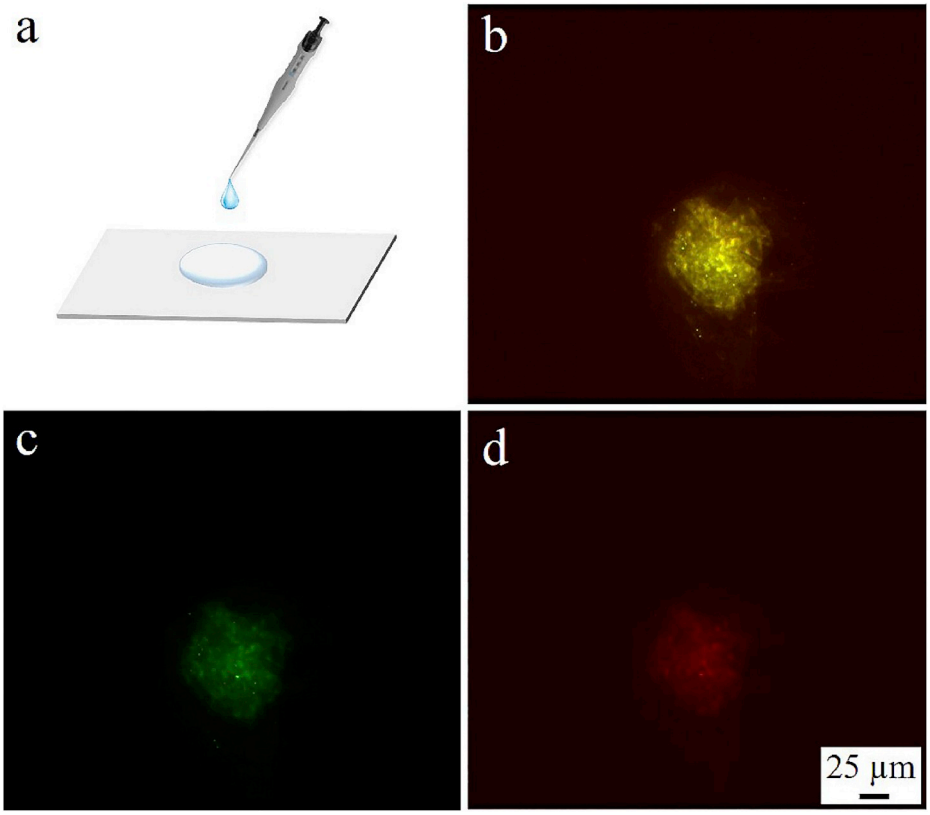

Fig. 5. FRET imaging of UCMFs. (a) Schematic demonstration of the sample (10 μL UCMF) preparation on glass cover slip. (b) FRET signal from aggregated UCMF illuminated with 980 nm laser. (c) Only UCNPs signal (green channel) obtained from the FRET image (b). (d) Only mOrange FPs signal (red channel) obtained from the FRET image (b). (For interpretation of the references to colour in this figure legend, the reader is referred to the Web version of this article.)

3.3. Characterisation of mOrange FPs

Figure S3 (ESI) shows the purity and fluorescence spectra of mOrange FPs. Impure residues will obscure the emission characteristic of a FP (Huang et al., 2010). The most common method of analyzing the purity of an isolated protein is to use SDS-PAGE electrophoresis. The above-mentioned technique has the additional advantage to determine the molecular weight of a protein. From the electrophoretic study (Fig. S3a, ESI) we have calculated the purity of mOrange to be ~70% pure. These proteins show characteristic molecular weight of ~25 kDa (Shaner et al., 2004) as observed before. Fig. S3b shows the excitation and emission spectra of mOrange FPs. The excitation and emission maximum appears at 548, and 566 nm, respectively, matching previous reports (Huang et al., 2010; Shaner et al., 2004). The inset in Fig. S3b shows the purified mOrange FPs solution.

3.4. Spectroscopic FRET measurements of UCMF

Fig. 2 shows the spectroscopic FRET analysis of the UCMFs. From Fig. 2a, we can observe that the broad excitation spectrum range of the mOrange FPs (acceptor) is straddling the green emission band of Cit-UCNP (donor), satisfying one primary requirement of FRET (Gert-Jan Kremers and Davidson; Huang et al., 2010). Fig. 2b shows a comparison of the emission spectra of Cit-UCNPs, and UCMFs, illuminated with 980 nm laser. Clearly, the emission spectrum of Cit-UCNPs showed no component at 566 nm, which was only present, as an extended but weak shoulder, for the UCMFs due to the mOrange FPs. The 540 nm emission intensity (I_{540}) from the Er^{3+} in the UCNP overshadowed the 566 nm emission from the mOrange relegating it as a weak shoulder. However, we have deconvoluted both the emission spectrum to extract the contribution from the mOrange and show the significant differences between the two spectra (Fig. 2c and d). The UCNP emission could be deconvoluted into 4 clear peaks at 520, 528, 540, and 548 nm (Fig. 2c). The UCMF emission showed the additional contribution of the 566 nm emission originating from the mOrange (Fig. 2d). The excitation of mOrange being around 548 nm, this 566 nm emission, under 980 nm excitation, is only possible through FRET.

Fig. S4 shows the pH dependent fluorescence study of individual FRET donor Cit-UCNPs and acceptor mOrange FPs. The pH dependent emission spectra, and the variation of the intensity of the spectral components of Cit-UCNPs (in DI-water), illuminated with 980 nm laser, was found to be pH insensitive within 3.0–8.0 (Figs. S4a and b, ESI). In contrast, mOrange FPs have shown strong pH sensitivity for the 566 nm band (Figs. S4c and d). As the pH decreases (towards acidic environment), the excitation and emission strengths decreased. The slope of the variation was particularly strong between pH 5.0–8.0 indicating high pH sensitivity (Dennis et al., 2012), qualifying the mOrange as a pH indicator. The change in the mOrange emission, from strong to weak, with pH is also reversible as we show in a video (Video 1, ESI). Now, when the FRET probe is constructed using Cit-UCNPs, and mOrange FPs, pH dependent synergistic effects can be expected.

Fig. 3 shows the pH dependent spectroscopic FRET analysis of the UCMFs. As observed before, under acidic environment, the FPs are inactive and thus do not exhibit the absorption properties necessary for energy transfer (Fig. 3a). The inactive FPs could again be activated at high pH values. This process is reversible (Video 1, ESI), and should go on for several cycles if the UCMFs are stable without any loss of signal strength.

Fig. 3b–d represents the pH dependent FRET emission signals from the UCMF. Fig. 3b shows that the I_{540} of the UCNP is decreasing, and consequently, the I_{566} of the mOrange FPs is increasing with increasing pH, and vice versa. The changes in the emission can be enhanced when zoomed in (Fig. 3 c,d). Similar phenomena have been observed in other types of FRET probes (Arppe et al., 2014; Dennis et al., 2012; Li et al.,

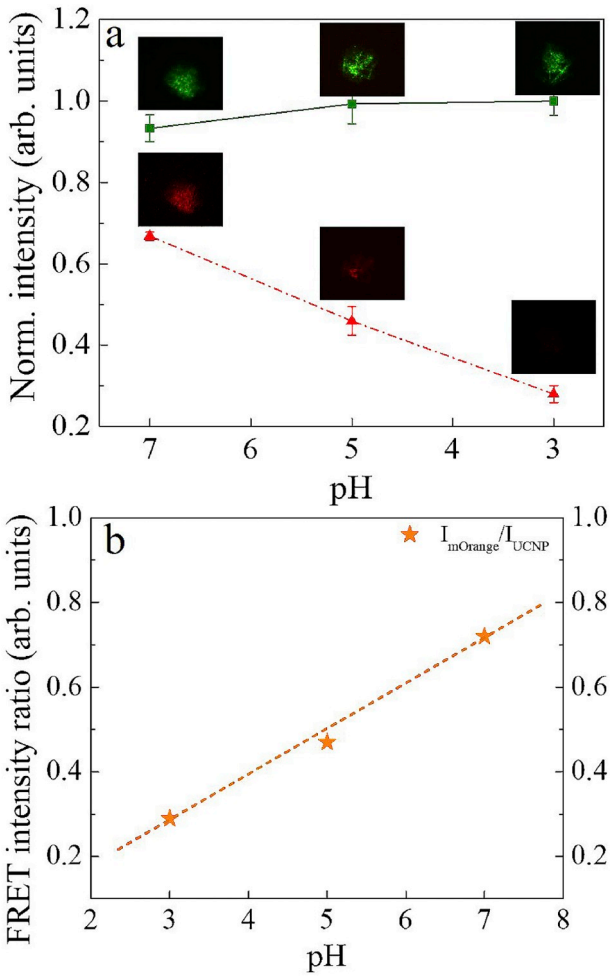

Fig. 6. pH dependent ratiometric FRET imaging. (a) FRET images of UCMF dispersed in different pH buffer (pH = 3–7), dropped on a glass cover slip, and their corresponding intensities measured by ImageJ software. The error bar indicates intensity values from at least five region of interests. The line joining the data points are just a guide to the eye only. (b) The FRET intensity ratio (mOrange FPs signal, in red channel, to UCNPs signal, in green channel) as a function of pH. The line joining the data points is a linear fit with adjacent R^2 = 0.98. (For interpretation of the references to colour in this figure legend, the reader is referred to the Web version of this article.)

2016).

One additional strength of these newly constructed UCMF probes is the emission at 655 nm, outside the absorption spectrum of the FP, that remains virtually unchanged with pH cycling. The constant I_{655} can be used as a reference, or normalization factor to understand and quantify any pH dependent spectral changes. Previous studies either showed ratiometric analysis, utilizing relative donor and acceptor emission that changes as a result of FRET at different pH, or self-ratiometric measurement involving the ratio between two signals of the same donor, one of which is affected by the FRET and the reference signal which is pH independent and is unaffected by FRET (Li et al., 2016). Interestingly, in our probe, we have both the ratiometric and self-ratiometric features because of the presence of the pH independent I_{655}. For these new class of probes, UCMF, both the I_{566}/I_{540} (ratiometric) and I_{540}/I_{655} (self--ratiometric) values can be plotted as a function of pH (Fig. 3e) to generate a reliable calibration line. Both the self-ratiometric and ratiometric variations yielded high R^2 linear fits indicating highly sensitive and accurate pH sensing (Li et al., 2016). The sensitivity of the pH measurement is given by the slope of the calibration curves (Fig. 3c). The sensitivity for the self-ratiometric, and ratiometric measurements are found to be 0.17, and 0.01 per unit variation of pH, respectively.

After the demonstration of FRET in the UCMFs, it is important to quantify the energy transfer efficiency (E) and the reversibility of the constructed probe. The FRET efficiency over the range of pH values can be calculated using the following equation (Dennis et al., 2012)

$$E = 1 - \frac{F_{DA}}{F_{DA}^{\cdot}} \quad (1)$$

where, F_{DA} is the donor emission at 540 nm of a conjugated probe at the given pH, and $F_{DA}^{\cdot}$ is the same donor emission at the most acidic pH measured, *i.e.*, when the energy transfer can be assumed to be minimal. Fig. 4a presents a maximum E of ~20% at pH values between 7 and 8. A low E ~0% was observed at pH = 3.0. QD based FRET probes have shown E values as high as 50% (Dennis et al., 2012) attributed to the high quantum yield in the one-photon absorbing fluorophores. However, the QDs require UV excitation which will induce strong background autofluorescence during FRET measurements. The UCMFs, on the other hand, show low quantum yield because of the multiphoton absorption. However, having 980 excitation for the UCMFs, the problems of autofluorescence and PD can be virtually ruled out. We have shown by Video 1 (ESI) the reversibility of the mOrange emission under cyclic pH change. Fig. 4b shows the pH reversibility of the UCMFs. The I_{566}/I_{540} ratios changed values from ~0.04 under pH = 8.0, to ~0.01 under pH = 3.0 and maintained these values for at least over 5 pH cycles. Such demonstration of probe parameter reversibility, with pH, matches with previously reported data (Li et al., 2016).

A comparison of the FRET probe (donor and acceptor) materials, the donor quantum yield, FRET efficiency, pH sensitivity by ratiometric and self-ratiometric analysis is provided in Table 1.

3.5. In-vitro FRET imaging, and pH estimation

In addition to spectroscopy, the UCMF probes must also pass the microscopic imaging tests to be qualified for intracellular pH sensing. Fig. 5 shows the FRET imaging of UCMFs dropped on a glass coverslip (Fig. 5a) and illuminated with 980 nm light. Fig. 5b shows the fluorescent overlaid FRET image of the aggregated UCMFs. Individual UCMFs cannot be resolved under the microscope objective. Individual signals from the Cit-UCNPs and the mOrange could be recorded in the green (Fig. 5c), and the red channel (Fig. 5d), respectively. The presence of these two emission signals under 980 nm excitation proves the FRET phenomenon in the probes. The fluorescence, and the FRET is thus established both by spectroscopy, and microscopic imaging.

Another confirmation of FRET could be obtained by photobleaching the acceptor molecules (Gert-Jan Kremers). Here, the mOrange FP is photobleached with prolonged 520–540 nm irradiation (monochromated Hg-lamp) and the UCNP donor emission is imaged under 980 nm excitation. The hypothesis is that as the mOrange emission decreases because of photobleaching, the green emission from the UCNP in the probe should increase. Fig. S5 represents the FRET validation study. Fig. S5a shows that the mOrange FPs are losing its brightness as a function of the photobleaching time while the green emission from the Cit-UCNPs increased. Later, we have measured the intensity from the images that are obtained, and the ratio of the green channel signal (UCNPs) to the red channel signal (mOrange) is plotted with time (Fig. S5b). The calculated ratio ($I_{mOrange}/I_{UCNP}$) is found to be decreasing with photobleaching time. The energy transfers between Cit-UCNPs and mOrange FPs is established.

In Fig. 6 we demonstrate pH dependent FRET imaging. At alkaline pH (7.0), where the energy transfer is maximum, we could observe the signal from both the donor and the acceptor (Fig. 6a). However, at a low pH (3.0), due to inefficient energy transfer, we could only observe the emission signal from Cit-UCNPs (Fig. 6a). We have taken 5 regions of interest (ROI), and measured the intensities at each ROI and then calculated the mean intensity with different pH values. To obtain a FRET

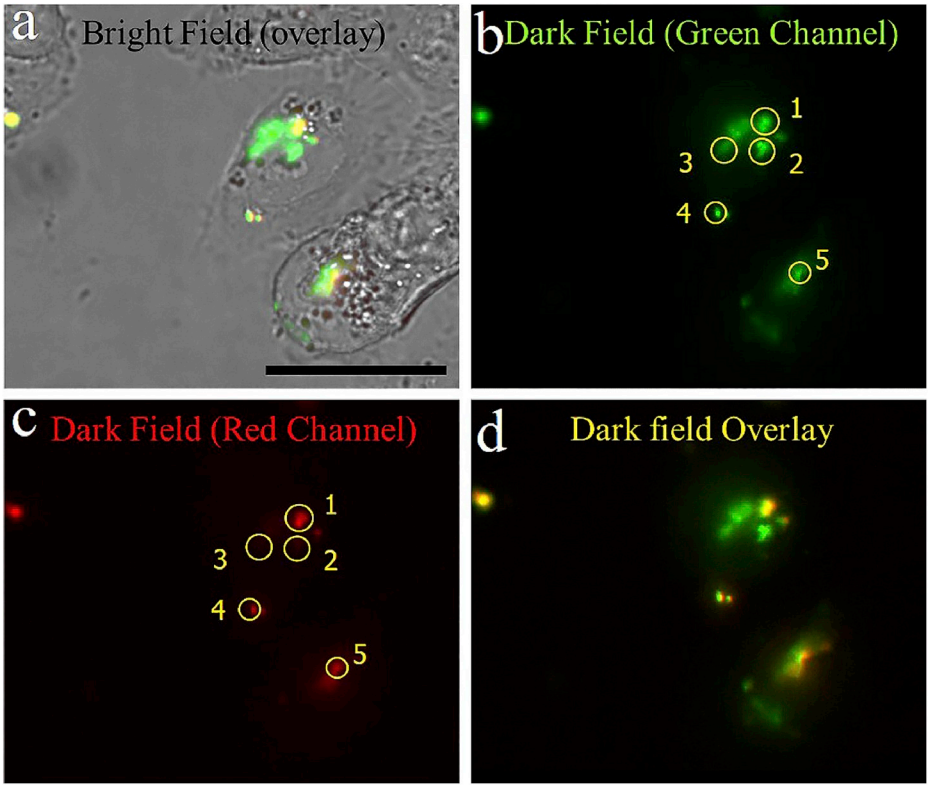

Fig. 7. In-vitro (in cell) FRET imaging of UCMF, internalised within HeLa cells. (a) Superimposed of bright field image with ratiometric FRET signals (excitation - 980 nm) of UCMFs localised in different cellular compartments of HeLa cells. (b) Only UCNPs signal obtained in green channel. (c) Only mOrange FPs signals obtained in red channel. (d) Overlaying FRET images containing both green channel and red channel signals. (For interpretation of the references to colour in this figure legend, the reader is referred to the Web version of this article.)

Table 2
FRET intensity ratio $I_{mOrange}/I_{UCNP}$ in different cellular compartment and corresponding pH range.

Region of Interest (ROI)	FRET ratios ($I_{mOrange}/I_{UCNP}$)	pH (Estimated from calibration curve)	Intracellular Organelles/Cytoplasm	Ref pH values
1	0.75	~7.2	Cytosol	6.8–7.2(Llopis et al., 1998)
2	0.25	~2.7	–	–
3	0.35	~3.6	Late endosomes/Lysosome	4.0–4.5 (Näreoja et al., 2017)
4	0.72	~7.0	Cytosol	6.8–7.2 (Llopis et al., 1998)
5	0.75	~7.2	Cytosol	

ratio calibration curve, we have plotted the mean intensity ratios between the acceptor signal ($I_{mOrange}$) and donor signal (I_{UCNP}) as a function of pH (Fig. 6b). The ratio $I_{mOrange}/I_{UCNP}$ was found to vary linearly with pH (Fig. 6b) as we have obtained spectroscopically also. The slope of the line (Fig. 6b) indicates the pH sensitivity of the FRET nanoprobes.

3.6. Cell cytotoxicity study of UCMF

For intracellular studies, biocompatibility of the UCMFs is a concern. We have performed the MTT assay (Chen et al., 2019) to investigate the biocompatibility of the UCMFs in HeLa cells. Figure S6a (ESI) represents the viability of the HeLa cells incubated with different concentrations of nanoprobes for 24 h. Cell viability is >80% even when the concentration of the UCMFs is as high as 400 ppm. Below this concentration (400 ppm), the UCMFs can be assumed to be biocompatible for the cells, and therefore suitable for pH sensing.

The internalization of these UCMFs, and its location in the cells, was confirmed by TEM. Figs. S6b–d (ESI) represents the UCMFs inside the HeLa cells which were incubated with 200 ppm of UCMFs. The TEM image confirms the presence of uptaken nanoparticles in the cytoplasm, and intracellular compartments such as endosomes and lysomes. Similar TEM results were also obtained in our previous studies with UCNPs in 3T3 cells (Gupta et al., 2018) and graphene oxide in B16F10 cells ((Kao et al., 2019).

3.7. Intracellular FRET based pH mapping

The constructed FRET nanoprobes, UCMFs, qualified for intracellular studies based on FRET efficiency exceeding 0.1%, and significant change in FRET ratio with pH (Campbell, 2009). To demonstrate the ability of UCMFs in intracellular pH sensing, we have carried out live-cell fluorescence imaging.

Fig. 7 represents the intracellular FRET imaging data. We incubated HeLa cells with UCMFs (200 ppm) for 24 h and washed (twice with PBS buffer) them to remove any uninternalized probes prior to imaging. The superimposed bright field overlay image in Fig. 7a shows the green, and yellow fluorescence of the UCMFs internalised by the HeLa cells. Fig. 7b and c shows the green channel (Cit-UCNPs), and the red channel signal (mOrange FPs), respectively. Fig. 7d shows the dark field overlaid FRET image. Clearly, when the green and red channel signals were present, simultaneously, the $I_{mOrange}/I_{UCNP}$ is low and the net fluorescence is yellow (ROI 1, 4, 5). When the green channel signal dominated, indicating high $I_{mOrange}/I_{UCNP}$, the overlaid signal is predominantly green (ROI 2, 3). Visually, we can consider that yellow ROIs indicate relatively alkaline, and the green ROIs are relatively acidic.

To estimate the precise pH values in the particular compartments where the UCMFs have accumulated, we have calculated the $I_{mOrange}/I_{UCNP}$ ratio, and inserted these values on the calibration curve (in Fig. 6b) and estimated the pH values. Table 2 shows the FRET intensity ratio in

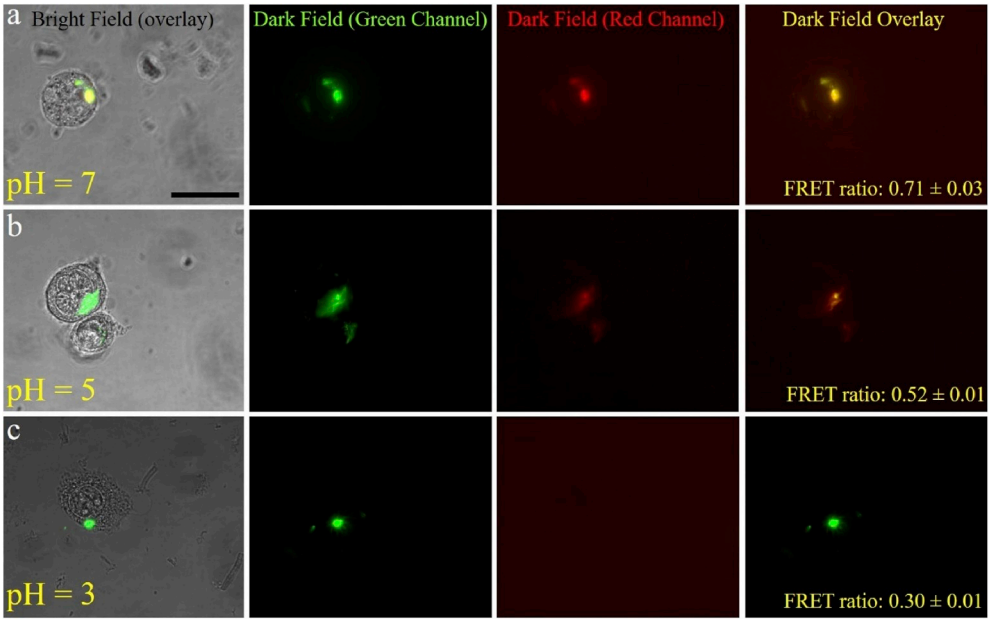

Fig. 8. Nigericin mediated in situ pH sensing in HeLa cells. Fluorescence imaging of UCMF internalised HeLa cell(s) with nigericin modulated pH of (a) 7.0, (b) 5.0, and (c) 3.0, respectively. From left to right (L to R): Bright field image, green (UCNP) channel, red (mOrange) channel, and dark field overlay of the red and green channel images. The FRET intensity ratio (red to the green channel) is mentioned in each dark field overlay panel. The standard deviations in the FRET ratios were obtained from four independent measurements. Common scale bar of 10 μm. (For interpretation of the references to colour in this figure legend, the reader is referred to the Web version of this article.)

different ROIs, and their corresponding pH values. For instance in ROI 1, $I_{mOrange}/I_{UCNP}$ ~0.75, and the estimated pH value obtained is 7.2, which matches with the standard cytosolic pH value (Llopis et al., 1998). Similar values were obtained for ROI 4, 5. But for ROI 3, $I_{mOrange}/I_{UCNP}$ is ~0.35, corresponding to pH = 3.6 normally found in early/late endosomes (Näreoja et al., 2017). From the superimposed image we could also conclude that the UCMFs mostly accumulated in the cytosol and in the endosomes in this study. However, problems exist for ROI 2, where the estimated pH value is found to be ~2.7, which is abnormal for any cellular compartment (Dennis et al., 2012). This may occur as a result of an error in image collection and probably can be solved by collecting more images and then applying statistical analysis. The UCMF probes did provide a better resolution and features in intracellular pH sensing. For example, Tuomas et al. (Näreoja et al., 2017) and Cuixia et al. (Li et al., 2016) have done similar studies using pH-sensitive dyes as acceptor molecule which are unstable and less biocompatible than mOrange FPs (Alford et al., 2009; Dennis et al., 2012). Dennis et al., (2012) did use mOrange FPs a FRET acceptor, however, with QDs as donor, which normally requires shallow penetrating UV excitation, and could induce autofluorescence, and damage the cells. Many of these above-mentioned studies address the photostability and toxicity issue of the nanoprobes as critical. The UCMFs are free from such concerns. Therefore, intracellular pH sensing is possible by using these UCMFs which can be used in theranostics, to specifically address drug delivery/release issues, and cellular diagnostics for drug design.

3.8. *In situ calibration of intracellular pH*

Next, to demonstrate the sensitivity of the UCMF to estimate the intracellular pH we have used Nigericin to modulate the intracellular pH (Li et al., 2016; Näreoja et al., 2017). Here, instead of probing the cellular compartments, the homogeneous intracellular pH was probed with the UCMFs (Mindell, 2012).

Fig. 8 represents the FRET images of HeLa cells in buffers with different pH of 7, 5, and 3. The use of the ionophore, Nigericin, would ensure identical pH value inside the cells. At an alkaline pH of 7.0 (Fig. 8a), we could select and observe individual emission signals from both the UCNPs (green) and mOrange FPs (orange), from the UCMFs uptaken in the cells. The bright field overlay image shows the location of the UCMFs within the cell, and the dark field overlay shows a yellow integrated emission from the UCMFs. The FRET intensity ratio (red channel to green channel) obtained is 0.71 ± 0.03. This FRET ratio matches well with our previous calibration curve shown in Fig. 6b. For the case of mildly acidic pH (pH = 5.0, Fig. 8b) the FRET intensity ratio dropped as mOrange FPs loses their ability to absorb energy from the UCNPs, and thus resulting in decrease in red channel signal. At the high acidic pH (= 3.0, Fig. 8c), the FRET efficiency was very low to inhibit mOrange excitation, and the green channel signal dominated. This vanishingly small red channel signal resulted in the integrated emission (darkfield overlay) to be predominantly green coming from the UCNP's 540 nm emission. To obtain a standard deviation and accuracy of the pH controlled FRET ratio, as mentioned in Fig. 8, we have performed the FRET imaging for four independent measurements (Figs. S7–S9, ESI). The above results indicate that the UCMFs can be used for intracellular pH estimation with excellent reproducibility and accuracy.

4. Conclusions

In conclusion, we have constructed a highly sensitive FRET based nanoprobe (UCMFs), with upconversion nanoparticles (UCNPs) as the donor, and mOrange fluorescence proteins as the acceptor, for intracellular pH sensing. The UCNP excitation of 980 nm provides longer penetration depth, express minimum autofluorescence, and high photostability to enhance the pH probe performance. FRET has been confirmed both spectroscopically, and by fluorescence imaging. The FRET efficiency of the probes is ~20% at pH = 7.0. The emission intensity ratio, $I_{mOrange}/I_{UCNP}$, scales linearly with the pH of a solution. Specific values of the $I_{mOrange}/I_{UCNP}$ ratio could be maintained under repeated pH cycling between 3.0 (acidic), and 8.0 (alkaline) environment signifying reversibility of the probes. The UCNPs emit pH insensitive 650 nm light, and hence the nanoprobe can perform both self-ratiometric, and ratiometric measurements unlike most of the reported pH probes. HeLa cells show viability up to 80% even when incubated with 400 ppm of the probes for 24 h. The UCMF uptake in HeLa cells is demonstrated through 980 nm excited fluorescence microscopy and visualized by TEM study. Dual-channel imaging measurements for the donor and acceptor emission enables the calculation of the $I_{mOrange}/I_{UCNP}$ ratio (by ImageJ) and estimation of the pH of the intracellular compartments within which these probes accumulated. Intracellular pH was controlled at different values (3.0, 5.0, and 7.0) by the use of an ionophore Nigericin, and the pH was estimated from the FRET ratio (red channel to green channel signal) obtained from the imaging studies. The

FRET ratios obtained matched well with the pH calibration curve. These results show the efficacy, reproducibility, and stability of the UCMFs as intracellular pH probes that can be utilized in early detection of cancer and other pH malfunctions in cells.

Electronic Supporting Information

The Electronic Supporting Information (ESI) contains detail expression, amplification, and extraction protocol for mOrange FPs. The optical properties such as absorption, fluorescence of UCNPs, and fluorescent proteins is also provided. In addition, cytoxicity, time and pH dependent FRET images can also be found in ESI.

Declaration of competing interest

The authors declare that they have no known competing financial interests or personal relationships that could have appeared to influence the work reported in this paper.

CRediT authorship contribution statement

Sandip Ghosh: Conceptualization, Methodology, Formal analysis. **Yu-Fen Chang:** Methodology. **De-Ming Yang:** Methodology. **Surojit Chattopadhyay:** Supervision, Writing - review & editing, Formal analysis.

Acknowledgement

The authors acknowledge financial support from the Ministry of Science and Technology (MOST), Taiwan, under grant # 107-2112-M-010-003-MY3. The authors would like to acknolowdge Mr. Yi-Ying, PhD student in, National Yang-Ming University for assisting with the sample preparation for Bio-TEM study.

Appendix A. Supplementary data

Supplementary data to this article can be found online at https://doi.org/10.1016/j.bios.2020.112115.

References

Alford, R., Simpson, H.M., Duberman, J., Hill, G.C., Ogawa, M., Regino, C., Kobayashi, H., Choyke, P.L., 2009. Toxicity of organic fluorophores used in molecular imaging: literature review. Mol. Imag. 8 (6), 00031, 7290.2009.

Arppe, R., Näreoja, T., Nylund, S., Mattsson, L., Koho, S., Rosenholm, J.M., Soukka, T., Schäferling, M., 2014. Photon upconversion sensitized nanoprobes for sensing and imaging of pH. Nanoscale 6 (12), 6837–6843.

Boyer, J.-C., Manseau, M.-P., Murray, J.I., van Veggel, F.C.J.M., 2010. Surface modification of upconverting NaYF4 nanoparticles with PEG−Phosphate ligands for NIR (800 nm) biolabeling within the biological window. Langmuir 26 (2), 1157–1164.

Brewer, S.H., Glomm, W.R., Johnson, M.C., Knag, M.K., Franzen, S., 2005. Probing BSA binding to citrate-coated gold nanoparticles and surfaces. Langmuir 21 (20), 9303–9307.

Campbell, R.E., 2009. Fluorescent-protein-based biosensors: modulation of energy transfer as a design principle. Anal. Chem. 81 (15), 5972–5979.

Cao, T., Yang, T., Gao, Y., Yang, Y., Hu, H., Li, F., 2010. Water-soluble NaYF4:Yb/Er upconversion nanophosphors: synthesis, characteristics and application in bioimaging. Inorg. Chem. Commun. 13 (3), 392–394.

Chen, C.-C., Li, J.-J., Guo, N.-H., Chang, D.-Y., Wang, C.-Y., Chen, J.-T., Lin, W.-J., Chi, K.-H., Lee, Y.-J., Liu, R.-S., Chen, C.-L., Wang, H.-E., 2019. Evaluation of the biological behavior of a gold nanocore-encapsulated human serum albumin nanoparticle (Au@HSANP) in a CT-26 tumor/ascites mouse model after intravenous/intraperitoneal administration. Int. J. Mol. Sci. 20 (1), 217.

Chen, G., Qiu, H., Prasad, P.N., Chen, X., 2014a. Upconversion nanoparticles: design, nanochemistry, and applications in theranostics. Chem. Rev. 114 (10), 5161–5214.

Chen, N.-T., Cheng, S.-H., Liu, C.-P., Souris, S.J., Chen, C.-T., Mou, C.-Y., Lo, L.-W., 2012. Recent advances in nanoparticle-based förster resonance energy transfer for biosensing, molecular imaging and drug release profiling. Int. J. Mol. Sci. 13 (12).

Chen, Q., Wang, C., Cheng, L., He, W., Cheng, Z., Liu, Z., 2014b. Protein modified upconversion nanoparticles for imaging-guided combined photothermal and photodynamic therapy. Biomaterials 35 (9), 2915–2923.

Chiu, T.-Y., Yang, D.-M., 2012. Intracellular Pb2+ content monitoring using a protein-based Pb2+ indicator. Toxicol. Sci. 126 (2), 436–445.

Chun, J.S., Jacobson, B.S., 1993. Requirement for diacylglycerol and protein kinase C in HeLa cell-substratum adhesion and their feedback amplification of arachidonic acid production for optimum cell spreading. Mol. Biol. Cell 4 (3), 271–281.

Clark, H.A., Kopelman, R., Tjalkens, R., Philbert, M.A., 1999. Optical nanosensors for chemical analysis inside single living cells. 2. Sensors for pH and calcium and the intracellular application of PEBBLE sensors. Anal. Chem. 71 (21), 4837–4843.

Davies, T.A., Fine, R.E., Johnson, R.J., Levesque, C.A., Rathbun, W.H., Seetoo, K.F., Smith, S.J., Strohmeier, G., Volicer, L., Delva, L., Simons, E.R., 1993. Non-age related differences in thrombin responses by platelets from male patients with advanced Alzheimer's disease. Biochem. Biophys. Res. Commun. 194 (1), 537–543.

Dennis, A.M., Rhee, W.J., Sotto, D., Dublin, S.N., Bao, G., 2012. Quantum dot–fluorescent protein FRET probes for sensing intracellular pH. ACS Nano 6 (4), 2917–2924.

Duan, H., Nie, S., 2007. Cell-penetrating quantum dots based on multivalent and endosome-disrupting surface coatings. J. Am. Chem. Soc. 129 (11), 3333–3338.

Gert-Jan Kremers, D.W.P., and Michael W. Davidson, Basics of FRET Microscopy. Nikon MicrscopyU. URL: https://www.microscopyu.com/applications/fret/basics-of-fret-microscopy. (Last accessed- 27th February, 2020).

Golovina, V.A., Blaustein, M.P., 1997. Spatially and functionally distinct Ca2+ stores in sarcoplasmic and endoplasmic reticulum. Science 275 (5306), 1643.

Gottlieb, R.A., Dosanjh, A., 1996. Mutant cystic fibrosis transmembrane conductance regulator inhibits acidification and apoptosis in C127 cells: possible relevance to cystic fibrosis. Proc. Natl. Acad. Sci. Unit. States Am. 93 (8), 3587.

Gupta, A., Lam, C.W., Wu, C.T., Yang, D.-M., Chattopadhyay, S., 2018. Photothermal disintegration of 3T3 derived fat droplets by irradiated silica coated upconversion nanoparticles. Part. Part. Syst. Char. 35 (12), 1800294.

Han, J., Burgess, K., 2010. Fluorescent indicators for intracellular pH. Chem. Rev. 110 (5), 2709–2728.

Hu, H., Xiong, L., Zhou, J., Li, F., Cao, T., Huang, C., 2009. Multimodal-Luminescence core–shell nanocomposites for targeted imaging of tumor cells. Chem. Eur J. 15 (14), 3577–3584.

Huang, P.-C., Chiu, T.-Y., Wang, L.-C., Teng, H.-C., Kao, F.-J., Yang, D.-M., 2010. Visualization of the Orai1 homodimer and the functional coupling of orai1-STIM1 by live-cell fluorescence lifetime imaging. Microsc. Microanal. 16 (3), 313–326.

Huang, X., Han, S., Huang, W., Liu, X., 2013. Enhancing solar cell efficiency: the search for luminescent materials as spectral converters. Chem. Soc. Rev. 42 (1), 173–201.

Kao, F.-H., Akhtar, N., Chen, C.-C., Chen, H.Y., Thakur, M.K., Chen, Y.-Y., Chen, C.-L., Chattopadhyay, S., 2019. In vivo and in vitro demonstration of gold nanorod aided photothermal presoftening of B16F10 melanoma for efficient chemotherapy using doxorubicin loaded graphene oxide. ACS Appl. Bio Mater. 2 (1), 533–543.

Kellum, J.A., 2000. Determinants of blood pH in health and disease. Crit. Care 4 (1), 6.

Kneipp, J., Kneipp, H., Wittig, B., Kneipp, K., 2007. One- and two-photon excited optical pH probing for cells using surface-enhanced Raman and hyper-Raman nanosensors. Nano Lett. 7 (9), 2819–2823.

Lakowicz, J.R., 2006. Principles of Fluorescence Spectroscopy, third ed. Springer, US, pp. 1–23 (Chapter 1).

Li, C., Zuo, J., Zhang, L., Chang, Y., Zhang, Y., Tu, L., Liu, X., Xue, B., Li, Q., Zhao, H., Zhang, H., Kong, X., 2016. Accurate quantitative sensing of intracellular pH based on self-ratiometric upconversion luminescent nanoprobe. Sci. Rep. 6, 38617.

Liu, A., Yang, L., Verwegen, M., Reardon, D., Cornelissen, J.J.L.M., 2017. Construction of core-shell hybrid nanoparticles templated by virus-like particles. RSC Adv. 7 (89), 56328–56334.

Liu, C., Gao, Z., Zeng, J., Hou, Y., Fang, F., Li, Y., Qiao, R., Shen, L., Lei, H., Yang, W., Gao, M., 2013. Magnetic/upconversion fluorescent NaGdF4:Yb,Er nanoparticle-based dual-modal molecular probes for imaging tiny tumors in vivo. ACS Nano 7 (8), 7227–7240.

Llopis, J., McCaffery, J.M., Miyawaki, A., Farquhar, M.G., Tsien, R.Y., 1998. Measurement of cytosolic, mitochondrial, and Golgi pH in single living cells with green fluorescent proteins. Proc. Natl. Acad. Sci. Unit. States Am. 95 (12), 6803.

Loiselle, F.B., Casey, J.R., 2003. Measurement of intracellular pH. In: Yan, Q. (Ed.), Membrane Transporters: Methods and Protocols. Humana Press, Totowa, NJ, pp. 259–280.

Lü, Q., Li, A., Guo, F., Sun, L., Zhao, L., 2008. Experimental study on the surface modification of Y2O3:Tm3+/Yb3+nanoparticles to enhance upconversion fluorescence and weaken aggregation. Nanotechnology 19 (14), 145701.

Mindell, J.A., 2012. Lysosomal acidification mechanisms. Annu. Rev. Physiol. 74 (1), 69–86.

Näreoja, T., Deguchi, T., Christ, S., Peltomaa, R., Prabhakar, N., Fazeli, E., Perälä, N., Rosenholm, J.M., Arppe, R., Soukka, T., Schäferling, M., 2017. Ratiometric sensing and imaging of intracellular pH using polyethylenimine-coated photon upconversion nanoprobes. Anal. Chem. 89 (3), 1501–1508.

Sedlmeier, A., Gorris, H.H., 2015. Surface modification and characterization of photon-upconverting nanoparticles for bioanalytical applications. Chem. Soc. Rev. 44 (6), 1526–1560.

Shaner, N.C., Campbell, R.E., Steinbach, P.A., Giepmans, B.N.G., Palmer, A.E., Tsien, R. Y., 2004. Improved monomeric red, orange and yellow fluorescent proteins derived from Discosoma sp. red fluorescent protein. Nat. Biotechnol. 22 (12), 1567–1572.

Shi, W., Li, X., Ma, H., 2012. A tunable ratiometric pH sensor based on carbon nanodots for the quantitative measurement of the intracellular pH of whole cells. Angew. Chem. Int. Ed. 51 (26), 6432–6435.

Shu, X., Shaner, N.C., Yarbrough, C.A., Tsien, R.Y., Remington, S.J., 2006. Novel chromophores and buried charges control color in mFruits. Biochemistry 45 (32), 9639–9647.

Talley, C.E., Jusinski, L., Hollars, C.W., Lane, S.M., Huser, T., 2004. Intracellular pH sensors based on surface-enhanced Raman scattering. Anal. Chem. 76 (23), 7064–7068.
Toptygin, D., Savtchenko, R.S., Meadow, N.D., Roseman, S., Brand, L., 2002. Effect of the solvent refractive index on the excited-state lifetime of a single tryptophan residue in a protein. J. Phys. Chem. B 106 (14), 3724–3734.
Webb, B.A., Chimenti, M., Jacobson, M.P., Barber, D.L., 2011. Dysregulated pH: a perfect storm for cancer progression. Nat. Rev. Canc. 11, 671.
Wilhelm, S., Kaiser, M., Würth, C., Heiland, J., Carrillo-Carrion, C., Muhr, V., Wolfbeis, O.S., Parak, W.J., Resch-Genger, U., Hirsch, T., 2015. Water dispersible upconverting nanoparticles: effects of surface modification on their luminescence and colloidal stability. Nanoscale 7 (4), 1403–1410.
Wray, S., 1988. Smooth muscle intracellular pH: measurement, regulation, and function. Am. J. Physiol. Cell Physiol. 254 (2), C213–C225.
Wurtele, E.S., Nikolau, B.J., 2000. [26] - characterization of 3-methylcrotonyl-CoA carboxylase from plants. In: Harris, R.A., Sokatch, J.R. (Eds.), Methods in Enzymology. Academic Press, pp. 280–292.
Xu, Y., Meng, X., Liu, J., Zhu, S., Sun, L., Shi, L., 2016. New nanoplatforms based on upconversion nanoparticles and single-walled carbon nanohorns for sensitive detection of acute promyelocytic leukemia. RSC Adv. 6 (2), 1037–1041.
Yuli, I., Oplatka, A., 1987. Cytosolic acidification as an early transductory signal of human neutrophil chemotaxis. Science 235 (4786), 340.
Zhao, H., Xu, X., Diaz, J., Muallem, S., 1995. Na+, K+, and H+/HCO3− transport in submandibular salivary ducts: membrane localization OF transporters. J. Biol. Chem. 270 (33), 19599–19605.